

Variational Scarring in Open Two-Dimensional Quantum Dots

Fartash Chalangari ,¹ Joonas Keski-Rahkonen ,^{1,2,3} Simo Selinummi ,¹ and Esa Räsänen ¹

¹*Computational Physics Laboratory, Tampere University, P.O. Box 600, FI-33014 Tampere, Finland*

²*Department of Physics, Harvard University, Cambridge, Massachusetts 02138, USA*

³*Department of Chemistry and Chemical Biology,
Harvard University, Cambridge, Massachusetts 02138, USA*

(Dated: May 1, 2025)

Quantum scars have recently been directly visualized in graphene quantum dots (Nature **635**, 841 (2024)), revealing their resilience and influence on electron dynamics in mesoscopic systems. Here, we examine variational scarring in two-dimensional quantum dots and demonstrate that these states remain robust even in an open system. We show that controlled perturbations enable modulation of electronic transmission via scarred states, presenting a viable approach to tuning quantum transport. These findings provide insights into the role of scarring in mesoscopic transport and open pathways for experimental realization in quantum devices.

Quantum chaos – sometimes referred to as quantum chaology [1, 2] – explores the transition from quantum states to classical behavior, a topic of intense debate since the advent of quantum mechanics [3, 4]. While classical mechanics exhibits true chaos, quantum systems display signatures of chaotic behavior in distinct ways [5–8], such as characteristic spectral statistics, wavefunction scarring, and other non-ergodic phenomena. At the heart of this exploration lies the correspondence principle, which is intimately linked to longstanding questions regarding measurement and decoherence in quantum mechanics [9, 10]. One proposed framework for understanding the emergence of classicality is quantum Darwinism, which posits that decoherence – by suppressing most quantum superpositions – yields environment-induced superselection (*einselection*). This process favors the survival of robust, *pointer states* that proliferate their information into the environment, while fragile quantum states are suppressed [11]. Intriguingly, these pointer states often exhibit quantum scarring, thus defying the expected ergodic behavior of quantum-chaotic systems [12].

Among the most striking manifestations of quantum chaos are scars [13], where certain eigenstates exhibit enhanced probability density along moderately unstable classical periodic orbits (POs). On the classical side, there is no direct counterpart for quantum scars which represent non-ergodic states allowed by the quantum ergodicity theorems [14–16]. Quantum scars have been supported by vast theoretical evidence [17–27], and have experimentally verified across a range of simulations and wave-analog experiments [28–41], culminating in the most recent direct observation of scarred eigenstates in a graphene-based quantum dot via a scanning tunneling microscopy [42].

In general, open quantum dots (QDs) provide a versatile platform for investigating quantum scars, offering valuable insights into classical-quantum correspondence partially due to their mixed classical phase space structure. While a single scarred state is typically thought to

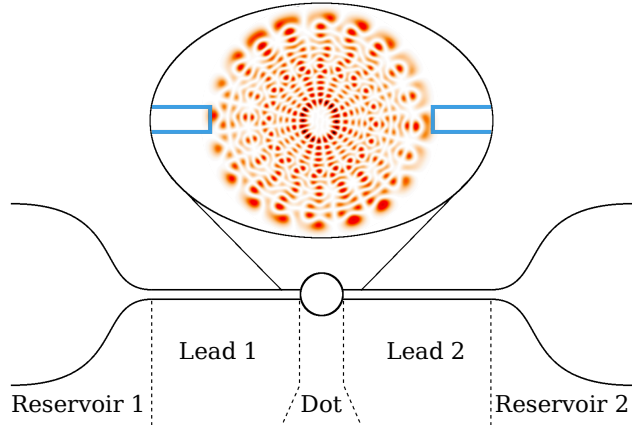


FIG. 1. Schematic of the quantum transport setup: A quantum dot serves as the central scattering region, weakly coupled to two leads that are connected to electron reservoirs with different electrochemical potentials.

be fragile against strong perturbations, such as system opening, the proliferation of scars can, however, result in significant robustness for the entire family of scarred states within a moderate energy window. Consequently, these scars can have a substantial effect on the transmission properties of quantum devices [29, 33, 43, 44]: notable transmission variations over small energy scales have been observed, with the fractal conductance fluctuations in quantum devices often attributed to their chaotic nature.

In this Letter, we investigate the quantum transport of a two-dimensional (2D) device illustrated in Fig. 1 in which the coupling to the reservoirs is mediated by a pair of quantum point contacts. We assume that the QD contains impurities introducing randomly positioned bumps within the confining potential, whereas a more controlled, localized disturbance is generated via a nanotip. In particular, the perturbation gives rise to a recently discovered form of scarring within the closed QD [45–51]: these scars emerge in a synthesis of the quantum near-

degeneracy in the unperturbed system and the localized nature of the perturbation. This unique birth mechanism [48] sets the variational scars apart from the conventional, Heller-type scarring [13, 17, 18], extending the concept of scarring into systems lacking suitable classical POs or when those orbits are too unstable to sustain conventional scarring. In other words, this origin allows scars to emerge and thrive under conditions that would typically inhibit conventional scarring. Furthermore, it highlights the fact that the near-degeneracies of a system can have a profound impact, not only the exact degeneracies associated with the continuous symmetries, as well as underscores the subtle role that disorder can play in a quantum device.

In particular, we here demonstrate that variational scars not only persist but also leave a distinct signature in the quantum transmission of an open QD, a fascinating prospect that has remained largely unexplored. We further support this finding by correlating the observed transmission peaks with a local density of states bearing the imprint of a scar, thus paving the way towards a very first experimental observation and successive utilization of variational scarring in a QD device.

A common strategy to realize a QD is to apply depletion potentials to lithographically defined gates [52, 53], which provide lateral confinement for a quasi-2D electron gas formed at the interface of a semiconductor heterostructure [54, 55]. Theoretical and experimental studies have validated the usage of anharmonic potentials to model the external confinement of electrons in QDs [56–62], even extending to the quantum Hall regime under strong magnetic fields [63–65], with experimental evidence of scars accumulating across a wide range of systems [28–41]. Moreover, the influence of external impurities on QDs has been quantitatively identified through differential magnetoconductance, which reveal the quantum eigenstates [46, 66, 67].

More specifically, our device studied here constitutes a QD coupled to two electron reservoirs with distinct electrochemical potentials, serving as source and drain, mediated by a pair of quantum point contacts modeled as leads, as shown in Fig. 1. Throughout the discussion, all values and equations are given in (effective) atomic units (a.u.), which can be converted to SI units by considering the material parameters for, e.g., GaAs. The single-electron Hamiltonian for the closed QD device is expressed as

$$H = \frac{1}{2}\nabla^2 + V_{\text{ext}} + V_{\text{tip}} + V_{\text{imp}}, \quad (1)$$

where $V_{\text{ext}} = \frac{1}{2}r^2 + \frac{1}{4}r^3$ is the anharmonic oscillator external confinement potential, in which the cubic term reflects the deviations from the harmonic confinement approximation taking place at higher energies, and subsequently breaks the special degeneracy structure of harmonic oscillator. Nevertheless, due to the circular sym-

metry, the eigenstates of the unperturbed system are labeled by two quantum numbers (r, m) , corresponding to radial and angular motions, respectively. While states $(r, \pm m)$ remain exactly degenerate, the system also exhibit near-degeneracies, called resonant sets that are associated with the POs of the classical counterpart. These POs can be enumerated directly; Each PO is connected to a resonance, where the oscillation frequencies of the radial and angular motion are commensurable.

In addition to the confining potential V_{ext} , recognizing that real quantum devices are often affected by disorder arising from impurities and imperfections – such as atoms or ions migrating into a QD system – we model the disorder potential as a sum of randomly distributed Gaussian bumps $V_{\text{imp}} = A_n \sum_i \exp(-\frac{|\mathbf{r}-\mathbf{r}_i|^2}{2\sigma_n^2})$, where A_n and σ_n represent the amplitude and width of the impurity bumps, respectively. This kind of disorder mode has been validated for a QD by density-functional theory [68, 69] and the diffusive quantum Monte-Carlo approach [62]. Moreover, we introduce a controllable localized perturbation stemming from a conducting nanotip for which a well-established approximation [70–72] is also the Gaussian profile $V_{\text{tip}} = A_T \exp(-\frac{|\mathbf{r}-\mathbf{r}_0|^2}{2\sigma_T^2})$, centered at the location \mathbf{r}_0 , where A_T and σ_T denote its amplitude and width.

Before delving into the transport properties of our device, we first briefly discuss the scarring phenomenon occurring in the closed QD described above. To compute the eigenstates of the QD defined by Eq.(1), we utilize the ITP2D software [73], which takes advantage of the imaginary time propagation method, particularly effective for 2D systems. As predicted by the scar theory [45, 48], a sufficient perturbation can give rise a distinct set of scarred eigenstates from a specific resonant set. Because these resonant states are linked to classical motion, certain linear combinations of these nearly-degenerate, unperturbed states create an interference pattern that traces out the path of a classical PO. While more complex scar geometries exist [45–48], we focus here on the simplest but also most ubiquitous form of variational scarring where the probability density condenses along an orbit associated with the classical bouncing motion. In essence, these *bouncing-ball* (BB) scars represent the quantum equivalent of radial, back-and-forth linear motion [51].

As a reference, we first consider the case where there is no nanotip (i.e., $V_{\text{tip}} = 0$), and the only perturbation comes from the impurity bumps V_{imp} , with amplitude $A_n = 2$ and width $\sigma_n \simeq 0.05$. In this scenario, we find that several states accommodate a BB scar. Within this impurity strength regime, the perturbation V_{imp} mostly leads to linear combinations of a single resonant set. Therefore, we can approximate the perturbed eigenstates employing the degenerate perturbation theory, i.e., by diagonalizing V_{imp} within the near-degenerate subspace

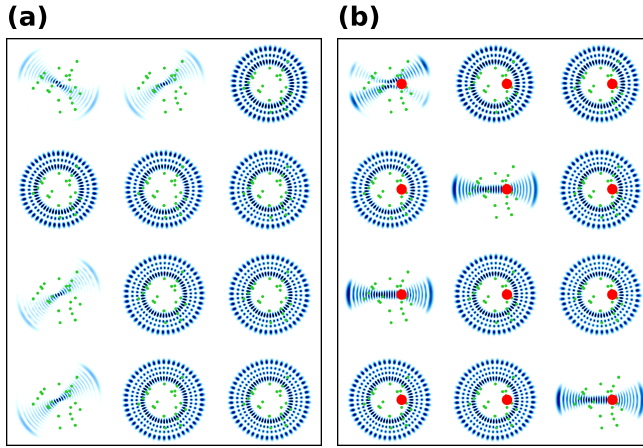


FIG. 2. (a) Examples of eigenstates in a closed, perturbed quantum dot containing random impurities (characterized by amplitude $A_n = 2$ and width $\sigma_n \simeq 0.05$). The positions of impurities are represented by green dots. (b) Examples of eigenstates with the same system and quantum numbers n as in (a), but now including a nanotip generating an additional, more prominent potential bump (amplitude $A_T = 12$, width $\sigma_T = 0.1$), which is indicated as a red dot.

of the given resonant set. According to the variational principle, these formed states are associated with the extrema of the expectation value of the perturbation. Due to the spatially localized nature of the perturbation, the scarred states are thus favored over non-scarred states whose probability density commonly covers a much larger region of space (see, e.g., Refs. [45, 48])

By the previous argument the scar orientations are mostly selected by the positions of the impurities resulting the most effective externalization of the perturbation: The BB scars shown in Fig. 2(a) orient themselves to maximize or minimize the perturbation by coinciding with or avoiding as many bumps as possible, respectively. While the scars maintain a similar alignment across a broad energy range, controlling the scar direction is challenging due to the inherent randomness of the impurity perturbation. However, by introducing an additional, stronger bump (i.e., $V_{tip} \neq 0$) via the nanotip ($A_T = 12$ and $\sigma_T = 0.1$), the BB scars align with the position of the nanotip, as seen in Fig. 2(b), which provides a feasible strategy to design the orientation of the scars experimentally. Furthermore, it is also worth noting that the single perturbation caused by the tip can be sufficient to generate distinct scars [46].

Previous work [45] has demonstrated variational scars to impact the transport characteristics of a QD by enabling wavepackets to propagate through the perturbed system with higher fidelity than in the corresponding unperturbed system. This boost in fidelity stems from the fact that there can be multiple strong scars oriented similarly within a moderate energy window. [45] Moreover, these scars are robust [47, 48, 51], further underscoring

their potential in a transport tool over the conventional scarring [13].

Nevertheless, the influence of these scars on the electrical transmission of an *open* quantum device has remained elusive. To address this question, we couple the QD to two leads, effectively opening the system. The leads are modeled as semi-infinite waveguides, with harmonic confinement in the transverse direction and free propagation along the longitudinal axis. This setup ensures smooth continuity and consistent boundary conditions at the interface with the scattering region. The coupling between the leads and the QD is characterized by the rate operator Γ , which reflects the level broadening induced by the reservoirs. To quantify the coupling strength, we define a dimensionless parameter $\mathcal{C} = \text{Tr}[\hat{\Gamma}(\omega)]/\delta$, where δ is the mean level spacing of the isolated QD in the energy window of interest. This ratio distinguishes between weak coupling ($\mathcal{C} \ll 1$), where transmission is dominated by sharp, isolated resonances, and intermediate to strong coupling ($\mathcal{C} \gtrsim 1$), where significant level broadening leads to overlapping resonances and more delocalized transport pathways.

The transmission through the QD is then determined within the Landauer-Büttiker formalism [74–76] as

$$\mathcal{T}(\omega) = \text{Tr}[\hat{G}^R(\omega) \hat{\Gamma}(\omega) \hat{G}^A(\omega) \hat{\Gamma}(\omega)], \quad (2)$$

which is computed by employing the TINIE software [77]. Moreover, we compute the local density of states (LDOS) as

$$\rho(\mathbf{r}, \omega) = -\text{Im}[\hat{G}^R(\mathbf{r}, \omega)], \quad (3)$$

revealing a map of the spatial distribution of quantum states contributing to the transport at specific probing energies ω .

In our transport setup, we choose to posit the tip strategically so that the induced BB scars oriented in conjunction to the leads and thus opening a direct pathway through the QD. In particular, we identify a prominent BB scarred state at energy 23.352 in the close system when exposed to the nanotip. To quantify its impact on electron transport, we focus on a bias voltage range of 23 – 24 and subsequently assess $\mathcal{T}(\omega)$ and $\rho(\mathbf{r}, \omega)$ with an energy resolution of $d\omega = 10^{-3}$ within this interval.

Figure 3 shows the transmission $\mathcal{T}(\omega)$ of the device as a function of energy ω in the weak coupling regime, i.e., $\mathcal{C} \ll 1$. As in the scarring analysis above, we compare two cases: one with only impurity disorder V_{imp} and coupling strength $\mathcal{C} \simeq 0.001$, and another with a nanotip also present, $V_{\text{imp}} + V_{\text{tip}}$, and $\mathcal{C} \simeq 0.002$. Notably, we observe significantly higher transmission peaks in the nanotip scenario [peak labeled (a) in Fig. 3] compared to the noise-only instance [peak labeled (b) in Fig. 3]. We attribute this boost in transmission to the presence of BB scarring, where the noise-only case lacks the coherent pathways formed by the lead-oriented scars. This

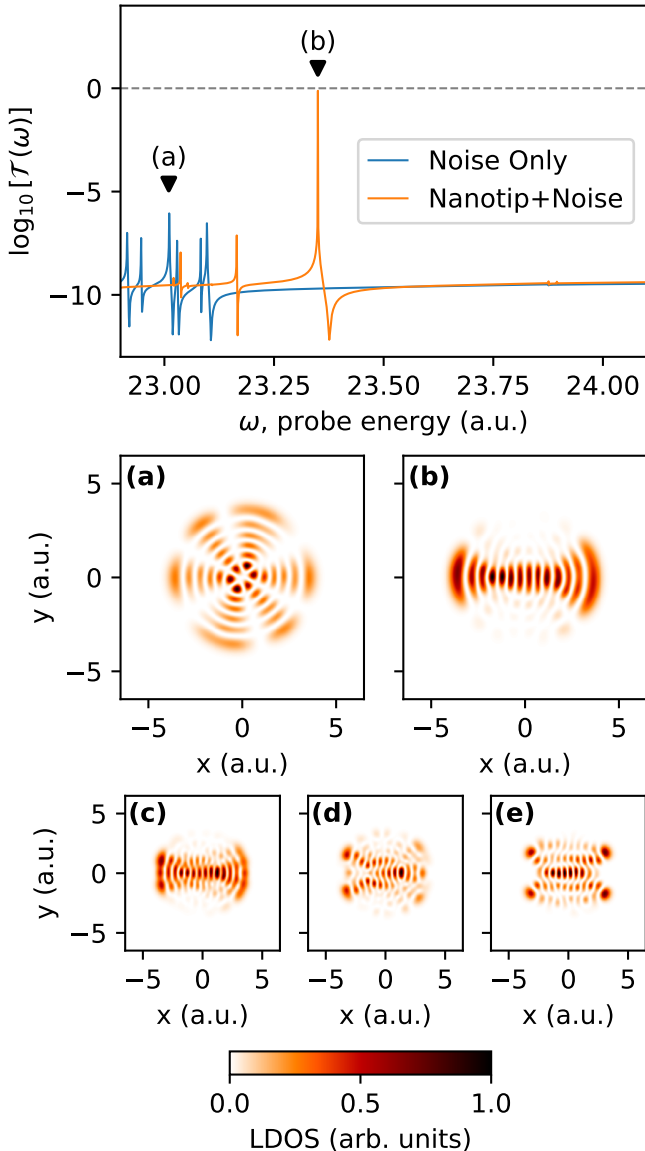


FIG. 3. Logarithm of transmission vs. probe energy within bias window 23–24 for noise-only case with $\mathcal{C} \simeq 0.001$ (blue) and nanotip+noise with $\mathcal{C} \simeq 0.002$ (orange), both in weak coupling limit ($\mathcal{C} \ll 1$). The strongest peaks are labeled as (a) for noise-only and (b) for nanotip+noise. Logarithmic scale is used due to the wide range of transmission values. Below, normalized LDOS is shown at the corresponding peak energies for (a) and (b), illustrating distinct bouncing-ball scar pattern induced by the tip. Panels (c)–(e) display normalized LDOS of nanotip+noise system at the energy corresponding to strongest transmission peak in weakly coupled leads ($\omega = 23.350$), now under stronger coupling strengths \mathcal{C} : (c) $\simeq 7.55$, (d) $\simeq 48.34$, and (e) $\simeq 121.20$.

interpretation is confirmed by the LDOS, which reveals a pattern at the transmission peak energy [Fig. 3(a)] corresponding to a BB scar of the closed QD, a feature absent in the nanotip-free benchmark [Fig. 3(b)].

On the other hand, panels (c)–(e) of Fig. 3 present

the LDOS for the nanotip case at the same energy of 23.350, corresponding to the strongest transmission peak in the weak coupling limit. These cases are associated with three different coupling strengths, $\mathcal{C} \simeq 7.55, 48.34, 121.20$, respectively, from intermediate to strong coupling limit. As the coupling strength increases, the LDOS pattern that initially exhibits a clear scar becomes gradually smeared and chaotic. This reflects the fact that stronger coupling results in greater self-energy, which in turn broadens QD's energy levels. The resulting spectral broadening diminishes the influence of individual scarred states on electron transport by delocalizing the transmission pathways.

To further explore the stronger coupling limit ($\mathcal{C} \gtrsim 1$), we focus on the same energy range where the nanotip-induced transport enhancements occur under weak coupling. Therefore, Fig. 4 shows the transmission for two cases of intermediate and strong couplings ($\mathcal{C} \simeq 12.21$ and $\mathcal{C} \simeq 96.59$). As illustrated in Fig. 4(a) and Fig. 4(b), the level broadening caused by the leads disrupts the scar patterns seen in the weak coupling regime, replacing them with more extended density distributions. Furthermore, this pronounced level broadening alters the line shape of the transmission peaks. In the weak coupling regime, the QD exhibits asymmetrical, Fano-like resonances [78, 79] in the transmission; whereas, in the stronger coupling case, the increased broadening of the QD energy levels smooths these resonances, resulting in more symmetric transmission peak profiles.

An intriguing direction for exploration is the use of a nanotip to orient the scars perpendicular to the leads. In this configuration, the scars would couple less effectively to the leads, allowing them to persist even in the strong coupling regime. However, this setup would invert the current situation, with the scars now associated with transmission dips rather than peaks. This effect could be interpreted as a consequence of antiscarring [50], leading to a reduced decay rate in the open system [80]. Furthermore, we anticipate that applying an external magnetic field [46] could offer additional control over scarring, potentially enabling scar-driven transport in more complex architectures, such as three-terminal devices.

On the experimental front, our study lays a foundation for further exploration in QD-based devices, where gate-defined potentials can replicate customized confinement, and precise impurity positioning can simulate nanotip perturbations. Inspired by recent advancements in mapping scars, scanning tunneling microscopy (STM) appears to be a viable option to verify the existence of variational scarring, as suggested in Ref. [81], paving a way to study these scars in open systems. Parallel to the STM path, our quantum device provides a robust platform for using scanning gate microscopy (SGM) as a direct method to probe scarred states in relation to the transmission: The SGM tip [82], biased to create a local perturbation by depleting electron density, allows

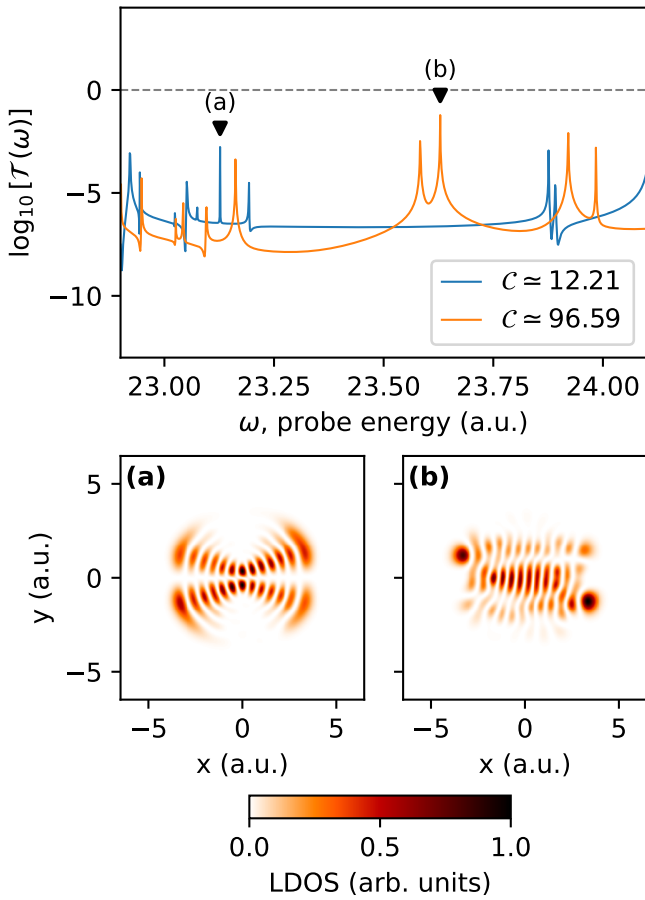


FIG. 4. Logarithm of transmission vs. probe energy within bias window 23–24, shown for intermediate ($\mathcal{C} \approx 12.21$, blue), and strong ($\mathcal{C} \approx 96.59$, orange) coupling strengths. Prominent transmissions labeled as (a) at $\omega = 23.127$ and (b) at energy $\omega = 23.629$. Below, the corresponding normalized LDOS at these peak energies reveals how increased self-energy disrupts the scarred patterns observed at weaker coupling, resulting in more extended wavefunction distributions.

for spatially resolved conductance investigations of a QD device [83].

To summarize, we investigated the influence of variational scarring on electron transport in two-dimensional quantum dots. In particular, we demonstrated that these scars not only survive but can also facilitate a controlled modulation of the transmission. In the weak coupling regime ($\mathcal{C} \ll 1$), scars enhance the transmission through the device, when oriented along the leads with a controlled perturbation, such as that generated by a nanotip. However, in the intermediate to strong coupling limit ($\mathcal{C} \gtrsim 1$), the effect of an individual scar is weakened by the non-scarred transport channels. Nevertheless, our study marks a step toward establishing a basis for further experimental exploration of this intriguing subclass of quantum scarring and harnessing its potential for nanoelectronic applications.

We acknowledge CSC—Finnish IT Center for Science for computational resources, and Research Council of Finland, ManyBody2D Project No. 349956, for financial support. J.K.-R. thanks the Oskar Huttunen Foundation for the financial support. This project is also supported by the National Science Foundation (Grant No. 2403491).

- [1] M. V. Berry, The bakerian lecture, 1987. quantum chaology, Proc. R. Soc. Lond. A413: 183–198 10.1098/rspa.1987.0109 (1987).
- [2] M. Berry, Quantum chaology, not quantum chaos, Physica Scripta **40**, 335 (1989).
- [3] A. Einstein, Zum quantensatz von sommerfeld und Epstein, Verh. Dtsch. Phys. Ges. **19**, 82 (1917).
- [4] A. D. Stone, Einstein’s unknown insight and the problem of quantizing chaos, Phys. Today **58**, 37 (2005).
- [5] E. J. Heller, *The Semiclassical Way to Dynamics and Spectroscopy* (Princeton University Press, 2018).
- [6] M. Gutzwiller, *Chaos in Classical and Quantum Mechanics*, Interdisciplinary Applied Mathematics (Springer New York, 1991).
- [7] G. Casati and T. Prosen, Quantum chaos, in *Statistical and Nonlinear Physics*, edited by B. Chakraborty (Springer US, New York, NY, 2022) pp. 561–573.
- [8] H.-J. Stöckmann, *Quantum Chaos: An Introduction* (Cambridge University Press, 1999).
- [9] S. Habib, K. Shizume, and W. H. Zurek, Decoherence, chaos, and the correspondence principle, Phys. Rev. Lett. **80**, 4361 (1998).
- [10] E. Joos and H. D. Zeh, The emergence of classical properties through interaction with the environment, Zeitschrift für Physik B Condensed Matter **59**, 223 (1985).
- [11] W. Zurek, Quantum darwinism, Nature Physics **5**, 181 (2009).
- [12] M. C. Gutzwiller, Periodic orbits and classical quantization conditions, J. Math. Phys. **12**, 343 (1971).
- [13] E. J. Heller, Bound-state eigenfunctions of classically chaotic hamiltonian systems: Scars of periodic orbits, Phys. Rev. Lett. **53**, 1515 (1984).
- [14] Y. Colin de Verdière, Ergodicité et fonctions propres du laplacien, Comm. Math. Phys. **102**, 497 (1985).
- [15] S. Zelditch, Uniform distribution of eigenfunctions on compact hyperbolic surfaces, Duke Math. J. **55**, 919 (1987).
- [16] A. I. Shnirel’man, Ergodic properties of eigenfunctions, Uspekhi Mat. Nauk **29**, 181 (1974).
- [17] L. Kaplan and E. J. Heller, Linear and nonlinear theory of eigenfunction scars, Ann. Phys. (N. Y.) **264**, 171 (1998).
- [18] L. Kaplan, Scars in quantum chaotic wavefunctions, Nonlinearity **12**, R1 (1999).
- [19] E. B. Bogomolny”, Smoothed wave functions of chaotic quantum systems, Physica D: Nonlinear Phenomena **31**, 169 (1988).
- [20] M. V. Berry, Quantum scars of classical closed orbits in phase space, Proc. R. Soc. Lond. A **423**, 219 (1989).
- [21] M. Kuś, J. Zakrzewski, and K. Życzkowski, Quantum scars on a sphere, Phys. Rev. A **43**, 4244 (1991).
- [22] G. M. D’Ariano, L. R. Evangelista, and M. Saraceno, Classical and quantum structures in the kicked-top

model, Phys. Rev. A **45**, 3646 (1992).

[23] S. Tomsovic and E. J. Heller, Semiclassical construction of chaotic eigenstates, Phys. Rev. Lett. **70**, 1405 (1993).

[24] F. Revuelta, E. Vergini, R. M. Benito, and F. Borondo, Short-periodic-orbit method for excited chaotic eigenfunctions, Phys. Rev. E **102**, 042210 (2020).

[25] O. Agam and S. Fishman, Quantum eigenfunctions in terms of periodic orbits of chaotic systems, J. Phys. A Math. **26**, 2113 (1993).

[26] O. Bohigas, S. Tomsovic, and D. Ullmo, Manifestations of classical phase space structures in quantum mechanics, Phys. rep. **223**, 43 (1993).

[27] D. A. Wisniacki, E. Vergini, R. M. Benito, and F. Borondo, Scarring by homoclinic and heteroclinic orbits, Phys. Rev. Lett. **97**, 094101 (2006).

[28] T. M. Fromhold, P. B. Wilkinson, F. W. Sheard, L. Eaves, J. Miao, and G. Edwards, Manifestations of classical chaos in the energy level spectrum of a quantum well, Phys. Rev. Lett. **75**, 1142 (1995).

[29] P. B. Wilkinson, T. M. Fromhold, L. Eaves, F. W. Sheard, N. Miura, and T. Takamasu, Observation of 'scarred' wavefunctions in a quantum well with chaotic electron dynamics, Nature (London) **380**, 608 (1996).

[30] E. E. Narimanov and A. D. Stone, Origin of strong scarring of wave functions in quantum wells in a tilted magnetic field, Phys. Rev. Lett. **80**, 49 (1998).

[31] A. Hönig and D. Wintgen, Spectral properties of strongly perturbed coulomb systems: Fluctuation properties, Phys. Rev. A **39**, 5642 (1989).

[32] E. Bogomolny, B. Dietz, T. Friedrich, M. Miski-Oglu, A. Richter, F. Schäfer, and C. Schmit, First experimental observation of superscars in a pseudointegrable barrier billiard, Phys. Rev. Lett. **97**, 254102 (2006).

[33] Y.-H. Kim, M. Barth, H.-J. Stöckmann, and J. P. Bird, Wave function scarring in open quantum dots: A microwave-billiard analog study, Phys. Rev. B **65**, 165317 (2002).

[34] H.-J. Stöckmann and J. Stein, "quantum" chaos in billiards studied by microwave absorption, Phys. Rev. Lett. **64**, 2215 (1990).

[35] U. Dörr, H.-J. Stöckmann, M. Barth, and U. Kuhl, Scarred and chaotic field distributions in a three-dimensional Sinai-microwave resonator, Phys. Rev. Lett. **80**, 1030 (1998).

[36] S. Sridhar, Experimental observation of scarred eigenfunctions of chaotic microwave cavities, Phys. Rev. Lett. **67**, 785 (1991).

[37] J. Stein and H.-J. Stöckmann, Experimental determination of billiard wave functions, Phys. Rev. Lett. **68**, 2867 (1992).

[38] J. Nöckel and A. Stone, Ray and wave chaos in asymmetric resonant optical cavities, Nature **385**, 45 (1997).

[39] S.-B. Lee, J.-H. Lee, J.-S. Chang, H.-J. Moon, S. W. Kim, and K. An, Observation of scarred modes in asymmetrically deformed microcylinder lasers, Phys. Rev. Lett. **88**, 033903 (2002).

[40] T. Harayama, T. Fukushima, P. Davis, P. O. Vaccaro, T. Miyasaka, T. Nishimura, and T. Aida, Lasing on scar modes in fully chaotic microcavities, Phys. Rev. E **67**, 015207(R) (2003).

[41] P. A. Chinnery and V. F. Humphrey, Experimental visualization of acoustic resonances within a stadium-shaped cavity, Phys. Rev. E **53**, 272 (1996).

[42] Z. Ge, A. Graf, J. Keski-Rahkonen, S. Slizovskiy, P. Poli, zogopoulos, T. Taniguchi, K. Watanabe, R. Van Haren, D. Lederman, V. Fal'ko, E. Heller, and J. Velasco, Direct visualization of relativistic quantum scars in graphene quantum dots, Nature **635**, 841 (2024).

[43] D. Wisniacki and G. G. Carlo, Scarring in open quantum systems, Phys. Rev. E **77**, 045201 (2008).

[44] D. Cabosart, A. Felten, N. Reckinger, A. Iordanescu, S. Toussaint, S. Faniel, and B. Hackens, Recurrent quantum scars in a mesoscopic graphene ring, Nano Lett. **17**, 1344 (2017).

[45] P. J. J. Luukko, B. Drury, A. Klales, L. Kaplan, E. J. Heller, and E. Räsänen, Strong quantum scarring by local impurities, Sci. Rep. **6**, 37656 (2016).

[46] J. Keski-Rahkonen, P. J. J. Luukko, L. Kaplan, E. J. Heller, and E. Räsänen, Controllable quantum scars in semiconductor quantum dots, Phys. Rev. B **96**, 094204 (2017).

[47] J. Keski-Rahkonen, P. J. J. Luukko, S. Åberg, and E. Räsänen, Effects of scarring on quantum chaos in disordered quantum wells, J. Phys.: Condens. Matter **31**, 105301 (2019).

[48] J. Keski-Rahkonen, A. Ruhanen, E. J. Heller, and E. Räsänen, Quantum lissajous scars, Phys. Rev. Lett. **123**, 214101 (2019).

[49] P. J. J. Luukko and J.-M. Rost, Polyatomic trilobite rydberg molecules in a dense random gas, Phys. Rev. Lett. **119**, 203001 (2017).

[50] J. Keski-Rahkonen, A. Graf, and E. Heller, Anti-scarring in chaotic quantum wells, arXiv preprint arXiv:2403.18081 (2024).

[51] S. Selinummi, J. Keski-Rahkonen, F. Chalangari, and E. Räsänen, Formation, prevalence, and stability of bouncing-ball quantum scars, Phys. Rev. B **110**, 235420 (2024).

[52] M. A. Kastner, The single-electron transistor, Rev. Mod. Phys. **64**, 849 (1992).

[53] S. M. Reimann and M. Manninen, Electronic structure of quantum dots, Rev. Mod. Phys. **74**, 1283 (2002).

[54] L. Kouwenhoven, Few-electron quantum dots, Rep. Prog. Phys. **64**, 10.1088/0034-4885/64/6/201 (2001).

[55] R. Hanson, L. P. Kouwenhoven, J. R. Petta, S. Tarucha, and L. M. K. Vandersypen, Spins in few-electron quantum dots, Rev. Mod. Phys. **79**, 1217 (2007).

[56] W. Fan, H. Zhang, and Z. Li, Unify the effect of anharmonicity in double-wells and anharmonic oscillators, International Journal of Theoretical Physics **63**, 10.1007/s10773-024-05774-w (2024).

[57] S. Sala, G. Zürn, T. Lompe, A. N. Wenz, S. Murmann, F. Serwane, S. Jochim, and A. Saenz, Coherent molecule formation in anharmonic potentials near confinement-induced resonances, Phys. Rev. Lett. **110**, 203202 (2013).

[58] M. Dineykhan, G. Efimov, G. Ganbold, and S. Nedelko, Anharmonic potentials, in *Oscillator Representation in Quantum Physics* (Springer Berlin Heidelberg, Berlin, Heidelberg, 1995) pp. 235–245.

[59] S. Schröter, P.-A. Hervieux, G. Manfredi, J. Eiglsperger, and J. Madroñero, Exact treatment of planar two-electron quantum dots: Effects of anharmonicity on the complexity, Phys. Rev. B **87**, 155413 (2013).

[60] V. Halonen, P. Hyvönen, P. Pietiläinen, and T. Chakraborty, Effects of scattering centers on the energy spectrum of a quantum dot, Phys. Rev. B **53**, 6971 (1996).

[61] E. Räsänen, J. Könemann, R. J. Haug, M. J. Puska, and

R. M. Nieminen, Impurity effects in quantum dots: Toward quantitative modeling, *Phys. Rev. B* **70**, 115308 (2004).

[62] A. D. Güçlü, J.-S. Wang, and H. Guo, Disordered quantum dots: A diffusion quantum monte carlo study, *Phys. Rev. B* **68**, 035304 (2003).

[63] S. Girvin and K. Yang, *Modern Condensed Matter Physics* (Cambridge University Press, 2019).

[64] M. Lei, N. Zhu, and H. Guo, Quantum hall effect in the presence of an antidot potential, *Phys. Rev. B* **52**, 16784 (1995).

[65] S. Baer and K. Ensslin, Quantum dots in the quantum hall regime, in *Transport Spectroscopy of Confined Fractional Quantum Hall Systems* (Springer International Publishing, Cham, 2015) pp. 233–246.

[66] H. Sari, E. Kasapoglu, S. Sakiroglu, I. Sökmen, and C. A. Duque, Effect of position-dependent effective mass on donor impurity- and exciton-related electronic and optical properties of 2d gaussian quantum dots, *The European Physical Journal Plus* **137**, 341 (2022).

[67] R. En-nadir, H. El-ghazi, M. Tihtih, W. Belaid, S. E. Zaki, I. Maouhoubi, and I. Zorkani, Analyzing the combined influences of external electric field, impurity-location, in-content, and qw's number on donor-impurity binding energy in multiple quantum wells with finite squared potential, *Optical and Quantum Electronics* **55**, 597 (2023).

[68] K. Hirose and N. S. Wingreen, Ground-state energy and spin in disordered quantum dots, *Phys. Rev. B* **65**, 193305 (2002).

[69] K. Hirose, F. Zhou, and N. S. Wingreen, Density-functional theory of spin-polarized disordered quantum dots, *Phys. Rev. B* **63**, 075301 (2001).

[70] A. C. Bleszynski, F. A. Zwanenburg, R. M. Westervelt, A. L. Roest, E. P. A. M. Bakkers, and L. P. Kouwenhoven, Scanned probe imaging of quantum dots inside inas nanowires, *Nano Lett.* **7**, 2559 (2007).

[71] E. E. Boyd, K. Storm, L. Samuelson, and R. M. Westervelt, Scanning gate imaging of quantum dots in 1d ultra-thin InAs/InP nanowires, *Nanotechnology* **22**, 185201 (2011).

[72] T. Blasi, M. F. Borunda, E. Räsänen, and E. J. Heller, Optimal local control of coherent dynamics in custom-made nanostructures, *Phys. Rev. B* **87**, 241303 (2013).

[73] P. Luukko and E. Räsänen, Imaginary time propagation code for large-scale two-dimensional eigenvalue problems in magnetic fields, *Computer physics communications* **184**, 769 (2013).

[74] M. Di Ventra, *Electrical Transport in Nanoscale Systems* (Cambridge University Press, 2008).

[75] G. Stefanucci and R. van Leeuwen, *Nonequilibrium Many-Body Theory of Quantum Systems* (Cambridge University Press, 2013).

[76] S. Datta, *Quantum Transport - Atom to Transistor* (Cambridge University Press, 2005).

[77] R. Duda, J. Keski-Rahkonen, J. Solanpää, and E. Räsänen, tinie – a software package for electronic transport through two-dimensional cavities in a magnetic field, *Comp. Phys. Comm* **270** (2022).

[78] U. Fano, Effects of configuration interaction on intensities and phase shifts, *Phys. Rev.* **124**, 1866 (1961).

[79] A. E. Miroshnichenko, S. Flach, and Y. S. Kivshar, Fano resonances in nanoscale structures, *Rev. Mod. Phys.* **82**, 2257 (2010).

[80] L. Kaplan, Scar and antiscar quantum effects in open chaotic systems, *Phys. Rev. E* **59**, 5325 (1999).

[81] J. Keski-Rahkonen, C. Zou, A. Graf, Q. Yao, T. Zhu, J. Velasco Jr, and E. Heller, Variational scarring in graphene quantum dots, arXiv preprint arXiv:2410.13157 (2024).

[82] L. Ousmane, Scanning gate microscopy response for local tip potentials beyond perturbation theory, *Phys. Rev. B* **108**, 195415 (2023).

[83] H. Sellier, On the imaging of electron transport in semiconductor quantum structures by scanning-gate microscopy: successes and limitations, *Semicond. Sci. Technol.* **26**, 10.1088/0268-1242/26/6/064008 (2011).